17èmes Journées Internationales de Thermique (JITH 2015)
*Marseille (France), 28 - 30 Octobre 2015*

# FLOW PATTERN IN AN EVAPORATING SESSILE DROP

Chafea Bouchenna[1,2a], Mebrouk Ait Saada[1b], Salah Chikh[1c], Lounès Tadrist[2d]
[1]USTHB, Faculty of Mechanical and Process Engineering, LTPMP, Alger 16111, Algeria
[2]Aix-Marseille Université, CNRS, Laboratoire IUSTI, UMR 7343, 13453 Marseille, France

[a]bouchennachafea@hotmail.fr, [b]m_aitsaada@yahoo.fr, [c]salahchikh@yahoo.fr, [d]ltadrist@polytech.univ-mrs.fr

**Abstract:** A numerical study of the evaporation of a water drop on a substrate at either room temperature or subject to higher temperature is carried out. The strong evaporation effect near the contact line, the thermo-capillarity and the thermal buoyancy effect are taken into account in modeling the convective flow within the drop. The mathematical formulation of the problem is based on the quasi-steady state conservation equations that govern the internal flow of the drop, the heat conduction in both solid and gas phases and the vapor diffusion in the surrounding air. The numerical results showed that the flow patterns inside the drop are strongly influenced by the substrate heating and thermal conductivity. Thermo-capillary effect is found to be the dominant one during a large period of drop lifetime. At the end of drop evaporation the flow is induced only by the mass loss near the contact line.

**Key words:** Evaporation, sessile drop, substrate, heat and mass transfer, flow pattern, thermo-capillary convection.

## 1. Introduction:

Despite the important number of studies about evaporating sessile droplets and controlling particle deposition in drying drops, the subject remains a topic that still attracts a high interest due to the evaporation which is a fundamental phenomenon in nature and has many applications in industry [1]. In particular, a better understanding of sessile drop dynamics during the evaporation is of capital interest for having more control over a large range of technological applications such as DNA mapping, thin film coating, ink-jet printing, electronic cooling and others. The flow inside the sessile droplet is induced by both non uniform evaporation rate along the liquid-gas interface [2-4], thermo-capillary effect (or thermal Marangoni effect) which is a result of the surface tension gradient at the droplet surface [6-8], and buoyancy effect due to liquid density gradient created by substrate heating [10]. The competition of these effects induces different flow pattern during droplet evaporation.

Deegan et al. [2] explained the formation of particle deposits near the contact line by the effect of a radial flow within an evaporating sessile drop. Dhavaleswarapu et al. [3] used microparticle image velocimetry measurements of the 3D flow field near the contact line to map the velocity field at very low contact angles. The velocity was found strongly influenced by the evaporation flux at the liquid-gas interface and to increase as the contact line is approached. Petsi and Burganos [4] carried out a numerical study to analyze the flow inside an evaporating sessile drop for any contact angle between 0 and 180°. In the case of pinned contact lines, the flow is directed towards the drop edge. In the case of receding contact lines, it is directed towards the center of the drop for contact angles less than 90°, whereas it is directed outwards for strongly hydrophobic substrates. Zhang et al. [5] showed the appearance of three different temperature distributions along the free surface of an evaporating sessile drop: for large contact angles, the surface temperature is dominated by the conduction path length and will then increase monotonically from the droplet center where the heat conduction path is the longest to the droplet edge where the conduction path is the shortest. Contrarily, for small contact angles, the evaporative cooling effect may be predominant, and the surface temperature then decreases monotonically from the apex where the evaporation rate is the lowest to the contact line where the evaporation rate is the highest. For the intermediate contact angles, the influence of the evaporative cooling and the conduction path are comparable. Hence, the surface temperature exhibits a non-monotonic spatial distribution which can induce different thermo-capillary flow patterns within the evaporating droplets. Xu and Luo [6] reported on the existence of a stagnation point on the drop surface where the flow changes its direction. At this point, the surface tension gradient and the

surface temperature gradient change their sign. Ristenpart et al. [7] established criteria for direction and magnitude of the liquid flow according to the contact angle and the ratio of substrate and liquid thermal conductivities. Bhardwaj et al. [8] showed different flow patterns caused by the competition of thermo-capillary and evaporation effects. The study of the liquid dynamics allowed determining the deposit shape to be either a ring-like pattern or a homogeneous bump. Tarasevich [9] considered a hemispherical drop at the very early stages of the evaporation process and showed that the capillary flow is insensitive to the ratio of the height to the contact radius of the drop. Lu et al. [10] have used the Grahshoff, Marangoni and Bond numbers to characterize the intensity of natural convection and Marangoni convection and their contribution inside an evaporating liquid drop on a heated solid surface. Prediction results show that both convections enhanced the evaporation rate, Marangoni convection produces the largest increase. Nakoryakov et al. [11] found that evaporation of different drops depends significantly on thermal inertia of material, wall thickness and the roughness of the heated wall. The drop lifetime is affected significantly by these factors.

In spite of the numerous investigations on sessile drop evaporation in heated or non-heated case, a better understanding of the mechanisms which control the flow patterns taking place in the drop and the induced temperature fields is still lacking. In this work, a phenomenological study of the convective flow inside a water sessile drop is investigated. A numerical model is developed by taking into account (i) the flow induced by the effect of the strong mass loss at the contact line, (ii) the thermo-capillary flow resulting from the effect of the surface tension gradient due to temperature variation at the drop surface and (iii) the flow due to the thermal buoyancy effect related to liquid density depending on the temperature. The objective is to analyze the flow resulting from the competition of these effects and temperature distribution in the drop for each flow structure. The effect of thermal properties of the substrate is also documented.

## 2. Mathematical formulation

Figure 1 illustrates the physical domain constituted with a symmetric drop of 10 $mm^3$ deposited on a cylindrical substrate of thickness $e_w$ = 1 mm, with a very large radius and a thermally insulated lateral face. The bottom surface of the substrate is maintained at a temperature higher than ambient temperature in the heated case. The surrounding air is at ambient temperature $T_\infty$= 25°C and relative humidity $H_a$ = 40%. The upper face of the substrate is covered by a very thin aluminum layer, which imposes to the drop an initial contact angle of 8°. The sessile drop has a spherical cap shape controlled by surface tension effect because its size (R=1.86mm) is lower than the capillary length $l=(\sigma/g.\rho_l)^{1/2}$ equal to 2.69 mm for water. The evaporation process occurs with a pinned contact line where the drop contact radius (R) is constant and the contact angle (θ) variable in time.

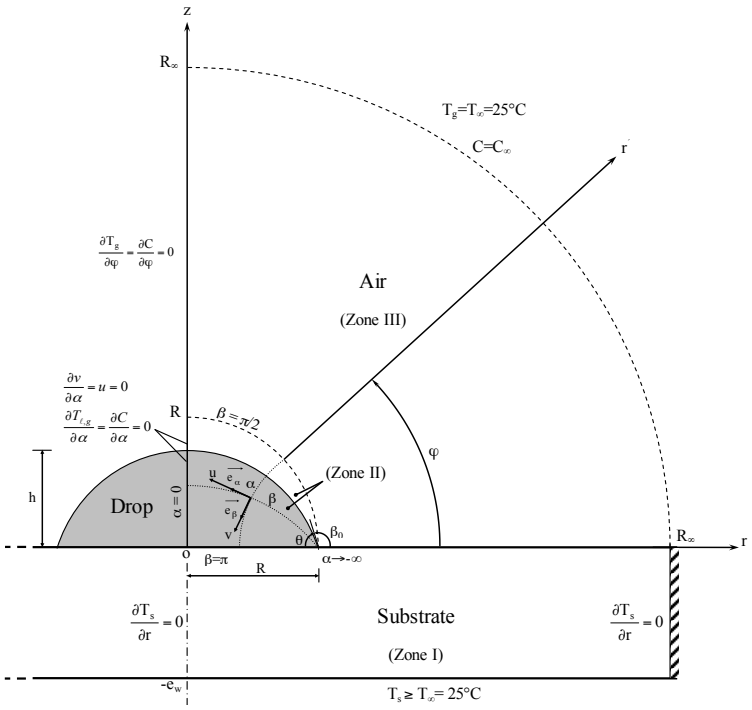


Figure 1 : Physical domain with boundary conditions.

The computational domain (Fig. 1) which encompasses $0 \le r \le R_\infty$ and $-e_w \le z \le R_\infty$ is divided in three zones: the solid substrate (zone I) meshed in cylindrical coordinates, the drop and its close surroundings (zone II) in toroidal coordinates and the outer surrounding air (zone III) in spherical coordinates. The choice of the coordinates system is dictated by the shape of the zone and its common boundary with other zones. The toroidal coordinates system is used in zone II because it allows better handling and localizing the moving liquid-air interface (a single value of the coordinate β is assigned to the interface) comparatively to other coordinates system where two coordinates are necessary. This yields more accurate numerical predictions of heat and mass exchanges at both sides of drop surface [12].

The physical problem is governed by continuity equation, Navier-Stokes equations and energy equation in the liquid phase. The heat transfer in both solid and gas phase occurs by conduction mode alone. The saturated vapor resulting from phase change at the liquid-gas interface is transferred by diffusion to ambient moist air. The velocity, temperature and concentration fields are assumed to be in quasi-steady state regime because of the slow motion of the liquid–gas interface during the evaporation [12]. The thermo-capillary effect in the drop is related to local variation of the surface tension with temperature at the drop surface: $\sigma = \sigma_\infty - (d\sigma/dT)(T - T_\infty)$, where $\sigma_\infty$ is the surface tension at $T_\infty$ and (dσ/dT) is the physical property of water. Boussinesq approximation is adopted for the temperature range between $T_\infty$ and $T_w$ ($T_\infty$= 25°C and $T_w$ varying between 25 and 50°C). Liquid density in the thermal buoyancy terms of Navier-Stokes equations varies linearly with temperature. Set in dimensionless form the equations governing the drop internal flow suggest taking the drop contact radius (R) as reference length and the characteristic thermo-capillary velocity $U_c = |d\sigma/dT|\,\Delta T/\mu_\ell$ at liquid-gas interface as reference velocity. The reference temperature difference ΔT is equal to ($T_w$ - $T_\infty$) in the case of a heated substrate and represents the drop cooling due to the evaporation in the case of a non-heated substrate (For $k_s >> k_\ell$: $\Delta T = D(1 - H_a)\,C_v(T_\infty)\,h_{\ell g}/k_\ell$ where $C_v$ is the vapor saturation concentration depending on the temperature). Thus, the governing equations in the liquid phase are written in dimensionless form as follows:

i. liquid phase:

$$\vec{\nabla}.\vec{W} = 0 \tag{1}$$

$$(\vec{W}.\vec{\nabla})\vec{W} = -\vec{\nabla}P + \frac{Pr}{Ma}\Delta\vec{W} - \frac{Pr}{Ma}Ra\,T_\ell^*\,\vec{I} \tag{2}$$

$$\vec{W}.\vec{\nabla}\,T_\ell^* = \frac{1}{Ma}\Delta T_\ell^* \tag{3}$$

$\vec{W}$ is the dimensionless velocity vector, $\vec{I}$ is the unit vector and $T_\ell^*$ the dimensionless temperature defined by: $T_\ell^* = (T_\ell - T_\infty)/\Delta T$. Three dimensionless numbers appear in these equations and constitute the study parameters of the problem: $Pr = (\nu/\alpha_T)_\ell$ is the Prandtl number, $Ra = g\beta_{T\ell}\Delta T\,R^3/(\nu\alpha_T)_\ell$ is the Rayleigh number and $Ma = |d\sigma/dT|\,\Delta T\,R/(\mu\alpha_T)_\ell$ is the Marangoni number. In the solid and gas phases, the quasi-steady state regime is also invoked. The surrounding air is assumed to be quiescent. Based on these considerations, the dimensionless governing equations are reduced to Laplace equations.

ii. in gas phase:

$$\Delta T_g^* = 0 \tag{4}$$

$$\Delta C^* = 0 \tag{5}$$

where the dimensionless concentration $C^*$ is defined by: $C^* = (C - C_\infty)/\Delta C$. The reference concentration difference ΔC or ($C_w$ - $C_\infty$) is equal to ($C_v(T_w)$- Ha $C_v(T_\infty)$) in the case of a heated substrate and ((1- Ha) $C_v$ ($T_\infty$)) in the case of a non-heated substrate.

iii. in solid phase:

$$\Delta T_s^* = 0 \tag{6}$$

The associated boundary conditions are indicated in Figure 1. Far from the drop, the fluid is quiescent and the concentration of the vapor is given by $C_\infty = H_a C_v(T_\infty)$. No temperature jump and continuity of heat and mass fluxes are applied at the interface between zones (II) and (III). Similar conditions are also imposed on the upper face of the substrate.

At the drop surface equations of mass balance, shear-stress balance and energy balance are given hereafter:

i. mass balance,

$$\left(\vec{W} - \vec{W}_I\right)\cdot\vec{n} = \frac{R^g_{\alpha_T}\left(\Delta C/\rho_\ell\right)}{Le\,Ma}\vec{J}^*\cdot\vec{n} \tag{7}$$

$\vec{n}$ is a normal unit vector, $\vec{W}_I\cdot\vec{n}$ is the dimensionless velocity of the moving interface and $\vec{W}\cdot\vec{n}$ is the velocity of a liquid particle. The dimensionless local evaporation flux $J^*$ is expressed according to Fick law by:

$$J^* = \frac{J}{D\,\Delta C/R} = -\frac{\partial C^*}{h^*_\beta\,\partial\beta}\bigg|_{\beta_0} \tag{8}$$

$h_\beta$ is the metric coefficient of the toroidal coordinate $\beta$ and D is the diffusion coefficient of water vapor in ambient air (D = 25 mm$^2$/s [13]). Three dimensionless numbers appear in eq. 7: the ratio $\Delta C/\rho_\ell$, the Lewis number, $Le = D/\alpha_{Tg}$, and the ratio of gas/liquid thermal diffusivity, $R^g_{\alpha_T} = \alpha_{Tg}/\alpha_{T\ell}$.

ii. Shear-stress balance,

$$\left(\vec{n}\,\bar{\bar{\tau}}\right)\cdot\vec{t} = \vec{\nabla}T^*\cdot\vec{t} \tag{9}$$

$\vec{t}$ is a tangential unit vector and $\bar{\bar{\tau}}$ is the dimensionless stress tensor. The dimensionless temperature gradient in the equation represents the term of thermo-capillary effect.

iii. Energy balance,

$$T^*_\ell = T^*_g \tag{10 a}$$

$$\frac{Ja}{Le}\left(\frac{\Delta C}{\rho_\ell}\right)J^* - \frac{\partial T^*_\ell}{h^*_\beta\partial\beta} + R^g_k\frac{\partial T^*_g}{h^*_\beta\partial\beta} = 0 \tag{10 b}$$

Equation (10 a) expresses the thermal equilibrium of both liquid and gas phases at the interface. In equation (10 b), $R^g_k = k_g/k_\ell$ is the ratio of gas/liquid thermal conductivity and $Ja = h_{\ell g}/(c_{p\ell}\Delta T)$ is the Jacob number where $h_{\ell g}$ is the evaporation latent heat.

A last interface condition must be given for fully formulating of the problem. Air at the drop surface is in a saturated state; its vapor concentration depends on temperature according to a polynomial relationship:

$$C_v(T) = \sum_{i=0}^{4} a_i T^i \tag{11}$$

The coefficients $a_i$ are chosen to fit experimental data of Raznjevic [14] and are given in [12]. With this condition and the other interface and boundary conditions as well as the governing equations in the three phases, the different velocity, temperature and concentration fields can be found based on the influencing parameters: Pr, Ra, Ma, $R_k$ (gas/liquid and solid/liquid), $R^g_{\alpha_T}$, Le, Ja and $\Delta C/\rho_\ell$. The concentration field is used to evaluate the evaporation rate in order to assess the lifetime of the drop. The dimensionless evaporation rate $\dot{M}^*$ over the whole drop surface is determined by:

$$\dot{M}^* = \frac{\dot{M}}{2\pi\, D\, R\, \Delta C} = -\int_0^{-\infty} \frac{\partial C^*}{h_\beta^* \partial\beta}\bigg|_{\beta_0} h_\phi^*\, h_\alpha^*\, d\alpha \qquad (12)$$

where $h_\alpha^*$, $h_\beta^*$ and $h_\phi^*$ are the dimensionless metric coefficients of the toroidal coordinates α, β and ϕ, respectively.

## 3. Numerical procedure:

The governing equations with the corresponding boundary and interface conditions are discretized by use of the control volume method [15]. Staggered grid with $N_\alpha \times N_\beta = 116 \times 104$ nodes and the SIMPLE algorithm are adopted to handle coupling between velocity and pressure fields in the liquid phase. A mesh step size of R/100000 is imposed around the contact line for accurate evaluation of the evaporation flux in this zone. A power law-differencing scheme (PLDS) is used to consider the contribution of convection and diffusion in the transport phenomena. The algebraic equations resulting from the finite volume discretization are solved using a combination of the tridiagonal matrix algorithm (TDMA) and the Gauss-Seidel iterative method along with under-relaxation. Solutions reach satisfactory convergence during the iterative process once the maximum relative error on the dependent variable (u, v, T, C) is lower than 0.1%. The maximum allowable absolute residue in the mass conservation equation is less than $10^{-10}$ and less than $10^{-5}$ in other conservative equations.

The implemented computation program is validated by comparison with results of previous works existing in the literature [12]. Another validation reveals a good qualitative agreement with the results of Yang et al. [1]. It is illustrated in Figure 2 which represents velocity field of both radial and thermo-capillary flow inside an evaporating water drop on a heated substrate for a contact angle of 50°. The flow named also radial flow in the case (i) is induced only by the effect of the privileged evaporation near the contact line. The cellular flow in the case (ii) is induced by the thermo-capillary effect combined with the evaporation effect.

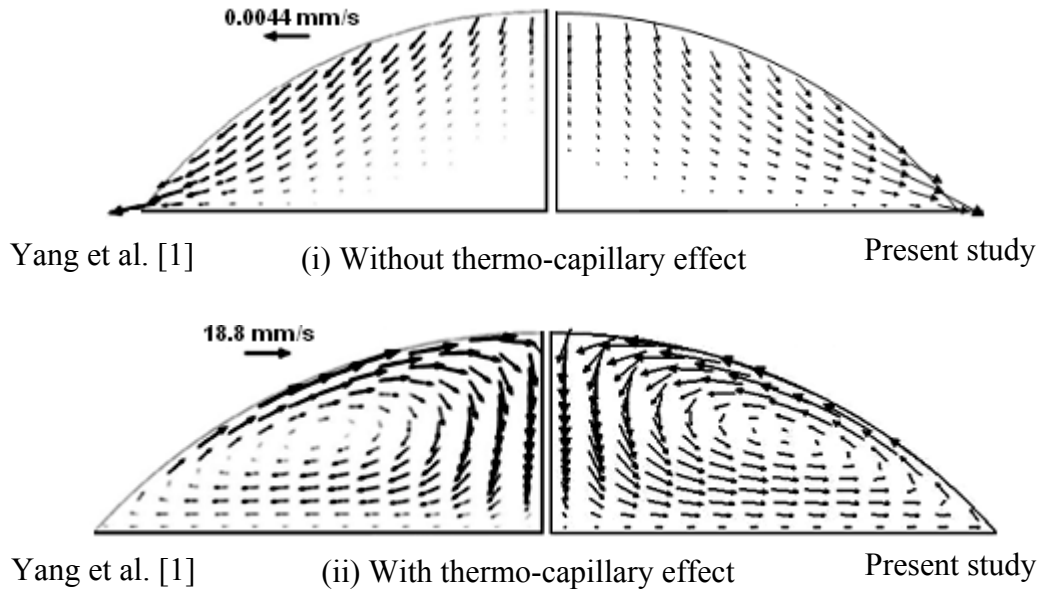


Figure 2 : Comparison with results of Yang et al. [1] for a contact angle of 50° (flow inside water sessile drop with R=1415µm, $\theta_0 = 50°$, $T_w = 50°C$, $T_\infty = 22°C$ and Ha = 50%, D=2.443m2/s, substrate of aluminum).

## 4. Results and discussion:

Internal flow of the evaporating drop may be induced by the non-uniform evaporation at the liquid-gas interface, the thermo-capillarity and the thermal buoyancy effect. The computation procedure used to show the importance of each effect during evaporation implies the application of three models. The first model considers only the evaporation effect, the second model introduces the thermo-capillary effect and the third model is completed by the thermal buoyancy effect. Based on these calculations, the thermal buoyancy is showed to have a negligible influence on the liquid motion. Thus, one can distinguish two cases: (i) flow without thermo-capillary effect and (ii) flow with thermo-capillary effect. The results presented in what follows are obtained for $25 \leq T_w \leq 50°C$ and $k_s = 0.25$ W/m K (PTFE) or 237 W/m K (aluminum).

Figure 3 represents different temperature profiles at the surface of an evaporating sessile drop on either a thermal conducting substrate or a thermal insulating substrate in heated and non heated cases. The flow pattern inside the drop is also given for each case. We observe that the substrate properties have a significant effect on the temperature gradient at the liquid-gas interface. For non-heated aluminum substrate case, the temperature gradient is monotonic and positive, so the coldest point is at drop apex. For large contact angles the flow is counterclockwise in the right part of the drop due to thermo-capillary effect induced by the negative surface tension gradient at the interface. At the evaporation end (very small contact angles) the flow becomes radial outward; this is due to the evaporation flux divergence at the contact line which must be compensated by liquid particles creating a radial flow. When the aluminum substrate is heated the two flow patterns found in non heated case exist also at high contact angles ($\geq 30°$) and the end of evaporation ($\leq 11°$), respectively. For the intermediate contact angles, the non monotonic surface tension gradient at the drop surface creates alternative recirculation cells. Their direction depends on temperature gradient. In the right part of the drop, we observe a clockwise recirculation in the zone where the surface temperature gradient is negative and a counterclockwise recirculation in the zone of positive one. The coldest point is in all cases at drop apex.

For non-heated PTFE substrate, the coldest point is always at drop apex and the temperature gradient is monotonic and positive at high contact angles. The thermo-capillary flow in this case is counterclockwise. During the evaporation, the coldest point approaches to the contact line so the temperature gradient becomes non-monotonic, and then there are two recirculation cells. The first cell at the drop edge is counterclockwise according to the positive temperature gradient in this region. It decreases in time and disappears at evaporation end. The second cell is clockwise and corresponds to negative temperature gradient. It becomes larger in time and dominates the flow at very low contact angles. When the PTFE substrate is heated, the flow pattern of alternative cells appears here too induced by the non-monotonic temperature gradient at the drop surface.

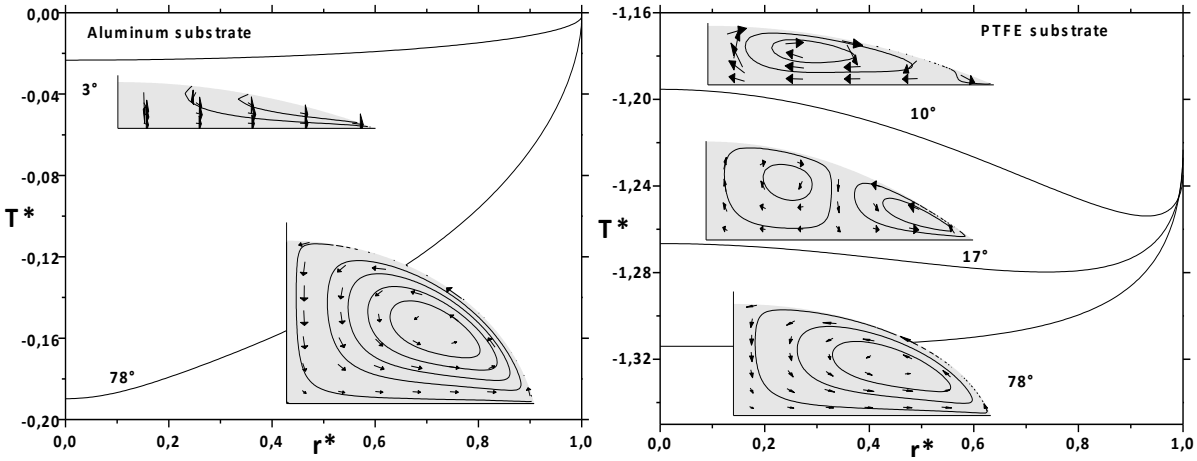


(a) Non heated substrate case ($T_w^* = 0$)

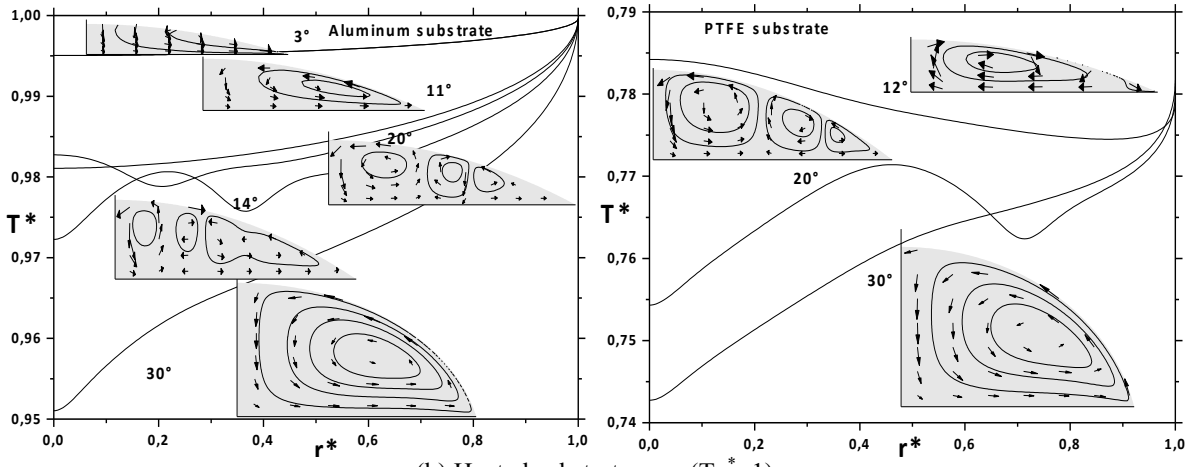


(b) Heated substrate case ($T_w^*$=1)

Figure 3: Flow pattern according to the temperature gradient at the drop surface for aluminum or PTFE substrates.

Figure 4 represents at left the maps giving the effect of the wall temperature on the flow pattern during the evaporation on a thermal conducting substrate, Fig. 4.a., or a thermal insulating substrate, Fig. 4.b. The beginning and the end of the flow pattern are given according to the dimensionless wall temperature $(T_w-T_\infty)/(T_{w\,max}-T_\infty)$ and the dimensionless time $t/t_f$ ($T_{w\,max}$ = 50°C, $t_f$ is the lifetime of the drop). Temperature field is also given to highlight the importance of the convective effects within the drop. In parallel, figure 4 gives at right the time variation of the Marangoni and Rayleigh numbers. These two dimensionless parameters are defined by:

$$Ma_s = Ma\ \Delta T_s / \Delta T \quad (13\ a)$$

$$Ra_h = Ra\ \Delta T_h\ h^3 / (\Delta T\ R^3) \quad (13\ b)$$

where $\Delta T_s$ is the maximal temperature difference along the liquid-gas interface and $\Delta T_h$ is the maximal temperature difference between the surface and the base of the drop during evaporation. Rayleigh and Marangoni numbers allow estimating the relative importance of the natural convection and the thermo-capillary convection within the evaporating drop. In all cases, the Rayleigh number is lower than the critical value $Ra_c$= 450 [10], so that the natural convection is negligible. Consequently, flow and heat transfer are influenced by the thermo-capillarity. For the aluminum substrate, Marangoni number is positive in both heated and non heated cases. For the PTFE substrate, it becomes negative towards the evaporation end where the flow is clockwise at right of the drop. Temperature distribution in the drop is dependent on the thermo-capillary flow pattern at high contact angles. In this case, the values of $Ma_s$ are higher than the critical value $Ma_c$ = 100 [10] and as a result the heat transfer is assured by Marangoni convection for most of the evaporation time. For low contact angles ($t/t_f$ > 0.8), there is no distortion of isotherms by the velocity field. We can deduce that the heat transfer within the drop is assured by conduction toward the evaporation end.

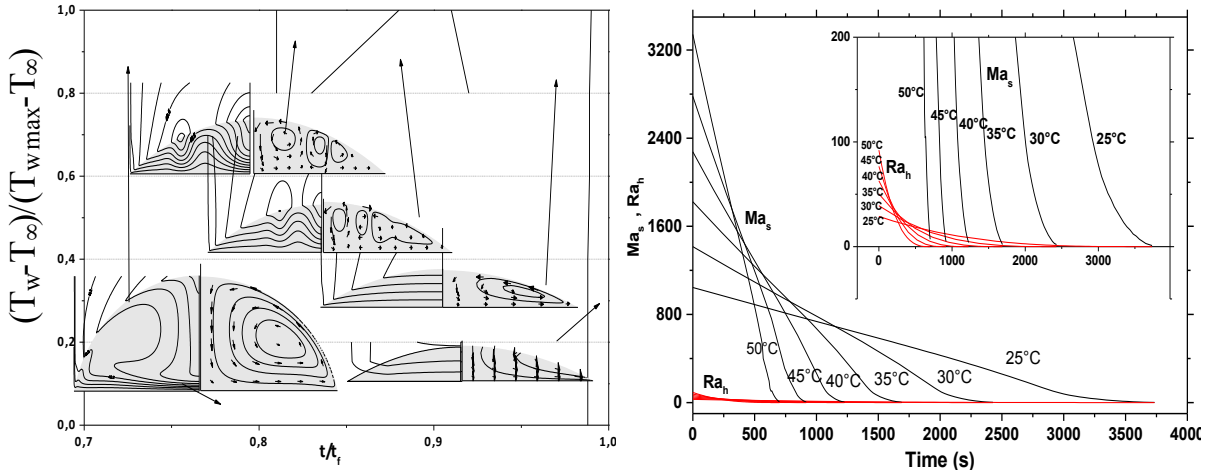


(a) Aluminum substrate

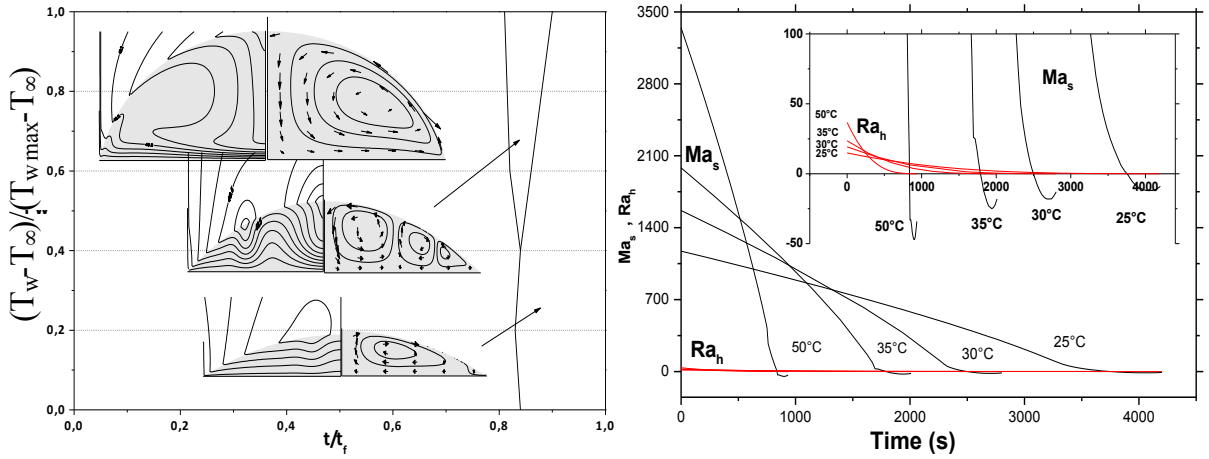


(b) PTFE substrate

Figure 4: Flow pattern maps (at left) and Marangoni and Rayleigh numbers (at right) for an evaporating water sessile drop.

## 5. Conclusion

A convection-diffusion model is developed to investigate numerically the flow and heat transfer inside an evaporating water drop on heated or non-heated substrates. The model takes into account the convective flow in the liquid phase, the heat conduction in both solid and gas phases and the vapor diffusion in the surrounding air. Several internal flow patterns are highlighted depending on the thermal conductivity and the heating temperature of the substrate. Based on the values of the Marangoni and Rayleigh numbers, the thermo-capillary effect on the flow is found to be the dominant one during the evaporation and can induce heat convection within the drop. At evaporation end, the flow is mainly influenced by the strong mass loss at the drop edge, but the heat transfer is dominated by the conduction mode.

**Nomenclature**

| | | |
|---|---|---|
| C | concentration | *(kg/m$^3$)* |
| $C_v$ | saturated vapor concentration | *(kg/m$^3$)* |
| D | vapor diffusion coefficient | *(m$^2$/s)* |
| $h_{\ell g}$ | latent heat of vaporization | *(J/kg)* |
| $H_a$ | relative humidity | *(% )* |
| J | evaporation flux | *(kg/m$^2$s)* |
| k | thermal conductivity | *(W/mK)* |
| $\dot{M}$ | evaporation rate | *(kg/s)* |
| R | contact radius | *(m)* |
| h | drop height | (m) |
| r, z | cylindrical coordinates | *(m)* |
| r , φ | spherical coordinates | *(m)* |
| T | temperature | *(°C)* |

| | | |
|---|---|---|
| $\vec{W}$ | dimensionless velocity vector | |
| *Greek Symbols* | | |
| α, β, ϕ | toroidal coordinates | *(rd)* |
| $\alpha_T$ | thermal diffusivity | *(m$^2$/s)* |
| ρ | densit | *(kg/m$^3$)* |
| μ | dynamic viscosity | *(kg/ms)* |
| θ | contact angle | *(°)* |
| ν | Kinetic viscosity | (m$^2$/s) |

*Subscripts*

| | |
|---|---|
| s, ℓ, g | solid, liquid, gas |
| ∞ | at infinity in surrounding air |
| * | dimensionless variable |

**Références**

[1] K. Yang, F. Hong, P. Cheng, A fully coupled numerical simulation of sessile droplet evaporation using Arbitrary Lagrangian–Eulerian formulation, *Int. J. Heat Mass Transfer* 70 409–420, (2014).

[2] R.D. Deegan, O. Bakajin, T.F. Dupont, G. Huber, R.S. Nagel, Contact line deposits in an evaporating drop, *Physical Review*, E 62, pp. 756-765, (2000).

[3] H. K. Dhavaleswarapu, Ch.P Migliaccio, S.V. Garimalla, J.Y. Murthy, Experimental investigation of evaporation from low contact angle sessile drops, Langmuir 26 880-888, (2010).

[4] J. Petsi and V.N. Burganos, Stokes flow inside an evaporating liquid line for any contact angle, J. *Physical Review* E78, 036324, (2008).

[5] K. Zhang, L. Ma, X. Xu, J. Luo, and D. Guo, Temperature distribution along the surface of evaporating droplets,J.*Physical Review* E89, 032404, (2014).

[6] X. Xu and J. Luo, Marangoni flow in an evaporating water droplet, *Appl. Phys. Lett.*, 91, 124102, 2007.

[7] W. D. Ristenpart, P.G. Kim, C. Domingues, J. Wan and H.A. Stone, Influence of substrate conductivity on circulation reversal in evaporating drops, J.*Phys.Rev.Lett.*99 234502, (2007).

[8] R. Bhardwaj, X. Fang and D. Attinger, Pattern formation during the evaporation of a colloidal nanoliter drop: a numerical and experimental study, J. *New Journal of Physics* 11 075020 , (2009).

[9] Y. Tarasevich, Simple analytical model of capillary flow in an evaporating sessile drop, J. *Physical Review*E71, 027301 s2005d, 2005.

[10] G. Lu, Y. Duan, X. Wang, D. Lee, Internal flow in evaporating droplet on heated solid surface, *Int. J. Heat Mass Transfer 5*4 4437-4447, (2011).

[11] V.E. Nakoryakov, S.Ya. Misyura, S.L. Elistratov, The behavior of water droplets on the heated surface. *J.of Heat and Mass Transfer* 55 6609–6617, (2012).

[12] M. Ait saada, S. Chikh, L. Tadrist, Evaporation of a sessile drop with pinned or receding contact line on a substrate with different thermophysical properties, *Int. J. Heat Mass Transfer* 58, 197–208, (2013).

[13] H. Hu and R.G. Larson, Analysis of the microfluid flow in an evaporating sessile droplet, *Langmuir*, 21, pp. 3963-3971*,* (2005).

[14] K. Raznjevic, Handbook of thermodynamic tables, Begell House, (1995).

[14] S.V. Patankar, Numerical heat transfer and fluid flow, McGrawHill, Hemisphere, (1980).